The frontotemporal dementia mutation R406W blocks tau's interaction with the membrane in an annexin A2–dependent manner

Anne Gauthier-Kemper,[1] Carina Weissmann,[1] Nataliya Golovyashkina,[1] Zsofia Sebö-Lemke,[3] Gerard Drewes,[4] Volker Gerke,[5] Jürgen J. Heinisch,[2] and Roland Brandt[1]

[1]Department of Neurobiology and [2]Department of Genetics, University of Osnabrück, 49076 Osnabrück, Germany
[3]Department of Neurobiology, University of Heidelberg, 69120 Heidelberg, Germany
[4]Cellzome AG, 69117 Heidelberg, Germany
[5]Institute of Medical Biochemistry, University of Münster, 48149 Münster, Germany

Changes of the microtubule-associated protein tau are central in Alzheimer's disease (AD) and frontotemporal dementia with Parkinsonism linked to chromosome 17 (FTDP-17). However, the functional consequence of the FTDP-17 tau mutation R406W, which causes a tauopathy clinically resembling AD, is not well understood. We find that the R406W mutation does not affect microtubule interaction but abolishes tau's membrane binding. Loss of binding is associated with decreased trapping at the tip of neurites and increased length fluctuations during process growth. Tandem affinity purification tag purification and mass spectrometry identify the calcium-regulated plasma membrane–binding protein annexin A2 (AnxA2) as a potential interaction partner of tau. Consistently, wild-type tau but not R406W tau interacts with AnxA2 in a heterologous yeast expression system. Sequestration of Ca^{2+} or knockdown of AnxA2 abolishes the differential trapping of wild-type and R406W tau. We suggest that the pathological effect of the R406W mutation is caused by impaired membrane binding, which involves a functional interaction with AnxA2 as a membrane–cytoskeleton linker.

Introduction

Frontotemporal dementia (FTD) is the second or third most common dementia after Alzheimer's disease (AD), and it comprises 3–10% of all neurodegenerative dementias (Yoshiyama et al., 2001). 30–50% of persons with FTD have a positive family history, and mutations in the microtubule-associated protein (MAP) tau are responsible for a large proportion of familial FTD cases. Several FTD cases have been linked genetically to chromosome 17q21-22 and have been referred to as "frontotemporal dementia and parkinsonism linked to chromosome 17" (Foster et al., 1997). According to a large population-based study in the Netherlands, three distinct mutations (G272V, P301L, and R406W) account for 16% of familial FTD cases (Rizzu et al., 1999).

Most families with FTDP-17 show deposits of tau in neurons or in glial cells. In some families, the tau deposits are identical to those present in AD (Spillantini et al., 1996) and consist of aggregates of hyperphosphorylated tau proteins in the cell soma. Why the MAP tau, which is normally enriched in the axon, redistributes to the somatodendritic compartment during disease is still a matter of debate. In AD, it has been shown that pathologically increased amounts of amyloid β (Aβ), a cleavage product of the amyloid precursor protein (APP), trigger an increased phosphorylation of tau (Busciglio et al., 1995; Leschik et al., 2007; Tackenberg and Brandt, 2009). Because hyperphosphorylated tau exhibits a reduced binding to microtubules, this may result in a loss of tau's axon-specific localization, thus triggering the pathological cascade.

The Rockefeller University Press $30.00
J. Cell Biol. Vol. 192 No. 4   647–661
www.jcb.org/cgi/doi/10.1083/jcb.201007161

JCB **647**

THE JOURNAL OF CELL BIOLOGY

With respect to the underlying molecular mechanism, the exonic FTDP-17 mutation R406W is most interesting because it causes an early onset tauopathy that clinically closely resembles AD and is often misdiagnosed as such (Ostojic et al., 2004; Ikeuchi et al., 2008; Lindquist et al., 2008). Why the R406W mutation leads to pathological changes in the absence of increased Aβ is unknown.

Overexpression of R406W tau in transgenic mice causes age-dependent accumulation of tau aggregates in neuronal perikarya, a reduction of the amount of tau in the axon, and induction of neurodegeneration (Zhang et al., 2004). All of these features have also been reported in AD mouse models (Götz and Ittner, 2008). However, in contrast to hyperphosphorylated tau in models of AD, the R406W mutation does not significantly alter the ability of tau to regulate microtubule dynamics (Bunker et al., 2006). This is consistent with the finding that soluble R406W tau from the brain of FTDP-17 patients is not hyperphosphorylated but is rather hypophosphorylated as compared with tau from healthy subjects (Miyasaka et al., 2001). Several studies also found that R406W tau does not differ from wild-type (wt) tau in its ability to form filaments in vitro (Aoyagi et al., 2007; Chang et al., 2008). These findings suggest that features other than the perturbation of microtubule binding or filament formation are responsible for the redistribution of R406W tau to the somatodendritic compartment in the development of tau pathology.

We have previously shown that tau binds to the axonal membrane cortex through its amino terminal projection domain (Brandt et al., 1995). Binding of tau to the membrane was sensitive to phosphorylation and was abolished after experimental hyperphosphorylation of tau (Maas et al., 2000; Eidenmüller et al., 2001). We have also provided evidence that tau is trapped in the distal axon mediated by its membrane binding. This trapping is abolished in the presence of Aβ or at increased tau phosphorylation (Weissmann et al., 2009). It can thus be hypothesized that the R406W mutation decreases the interaction of the mutant protein with the membrane much like an Aβ-induced tau hyperphosphorylation, thereby causing a loss of axonal localization.

To scrutinize functional consequences of the R406W mutation, we expressed epitope-tagged human tau constructs in neuronally differentiated PC12 cells. We determined the phosphorylation profile using a panel of phosphorylation-sensitive antibodies and analyzed tau distribution using fluorescence decay after photoactivation. Binding to the membrane cortex was determined by subcellular fractionation of surface-biotinylated cells, and potential tau interaction partners were identified by tandem affinity purification (TAP) tag purification and mass spectrometry (MS).

Results

To determine functional consequences of the FTDP-17 mutation R406W in the MAP tau, a panel of epitope-tagged human tau variants with or without the R406W mutation in the carboxy-terminal nonmicrotubule binding region were produced (Fig. 1). The constructs were based on the shortest isoform of tau coding for 352 aa and the longest human central nervous
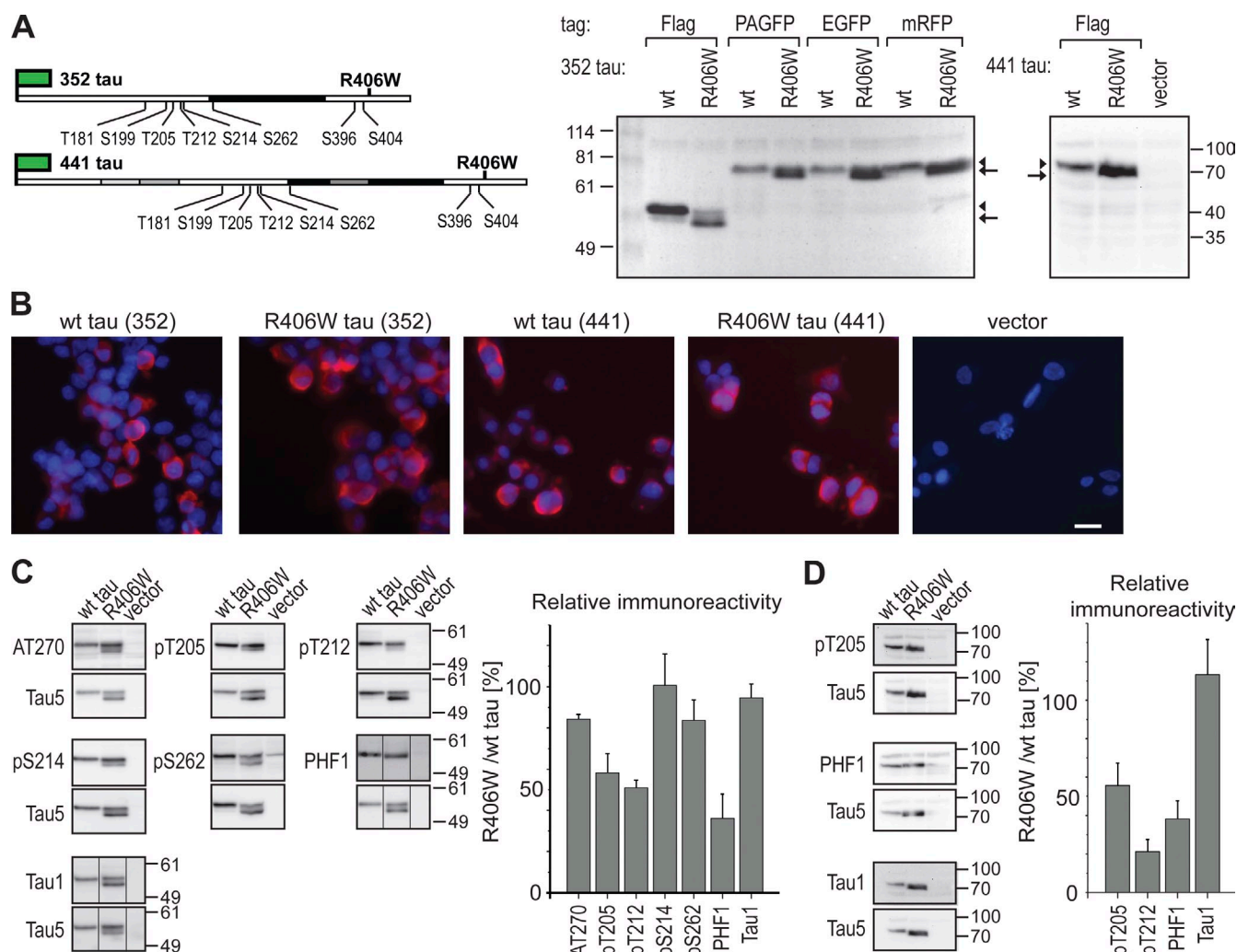
system isoform (441 aa) containing also the adult-specific exons 2, 3, and 10 (to allow for an easy reference to previous work, the numbering of the mutated site and the phosphorylation epitopes is based on the tau isoform containing 441 aa). For immunological detection and use in live cell imaging, the short (8 aa) FLAG-sequence and three longer fluorescent tags (EGFP, photoactivatable GFP [PAGFP], and mRFP) were used. The tags were fused to the amino termini of the tau variants because additional amino-terminal sequences do not interfere with the interaction of tau with microtubules or membrane components (Brandt et al., 1995; Maas et al., 2000).

The constructs were expressed in PC12 cells as a model for neural cells (Fig. 1 A; Greene et al., 1991). In immunoblots of lysates of transfected PC12 cells, the proteins separated at apparent molecular masses of 50–55 kD and 65–70 kD (FLAG-tagged 352 and 441 tau, respectively) and 75–80 kD (PAGFP-, EGFP-, and mRFP-tagged 352 tau). The electrophoretic mobility was lower than would be expected from the calculated molecular weight, which is in agreement with earlier studies (Maas et al., 2000; Weissmann et al., 2009). It was evident that wt tau separated as a single band, whereas the respective R406W mutated protein separated as a doublet, with one band having a higher electrophoretic mobility (Fig. 1 A, right, arrow versus arrowhead). This may indicate the presence of a population with reduced phosphorylation in R406W tau because it is known that phosphorylation leads to detergent-resistant conformational domains in tau protein, which result in decreased electrophoretic mobility. Transient or stable expression of the R406W mutant did not result in obvious phenotypic alterations of undifferentiated PC12 cells, and comparable amounts of the constructs were expressed (Fig. 1 B).

R406W tau exhibits reduced phosphorylation at several residues compared with wt tau including the PHF1 site (S396/404), T205, and T212

Tauopathies are thought to be associated with increased phosphorylation of tau protein (Stoothoff and Johnson, 2005). However, with respect to the R406W mutation, both increased and decreased phosphorylation of tau have been described depending on the cell system used (Krishnamurthy and Johnson, 2004).

To determine the effect of the R406W mutation on the phosphorylation profile of tau in PC12 cells, lysates of cells that stably expressed FLAG-tagged wt tau or R406W tau were analyzed by quantitative immunoblotting with phosphorylation-sensitive antibodies. As a loading control, blots were also stained with the phosphorylation-independent Tau5 antibody, which detects all tau isoforms (Fig. 1 C). Some of the phosphorylation-sensitive antibodies (pT205, pT212, pS214, and PHF1) preferentially detected the R406W tau band with the lower electrophoretic mobility (i.e., the upper band), which confirms that the reduced electrophoretic mobility of wt tau is caused by a higher phosphorylation state. No difference was observed with an antibody that detected a dephosphorylated epitope (Tau1). The quantification of all immunoreactive bands revealed that the R406W mutation exhibits a decreased phosphorylation at T205, T212, and the PHF1 epitope (S396/S404; reductions of

Figure 1. **Expression and phosphorylation of human wt and R406W mutated tau in neural PC12 cells.** (A) Schematic representation of the epitope-tagged tau fusion constructs and immunoblot of tau-expressing cells. The tag is indicated as a green flag, the microtubule-binding region (MBR) as black box. Adult-specific exons 2, 3, and 10 are indicated in gray. The R406W FTDP-17 mutation and some disease-relevant phosphorylation sites are indicated (numbering according to the longest central nervous system tau isoform containing 441 aa). The AT270 antibody recognizes phosphorylated T181, PHF1 phosphorylated S396/S404, and Tau1 dephosphorylated S199. Immunoblots of lysates detected with Tau5 antibody show separation of the fusion proteins at the expected size. Note that wt tau separates as a single band (arrowhead), whereas R406W mutant tau exhibits a doublet (arrowhead and arrow) indicative of the presence of a population with decreased phosphorylation. (B) Fluorescence micrographs of PC12 cells stably expressing different tau constructs and a vector control. Proteins were detected using monoclonal anti-FLAG antibody, and nuclei were stained with DAPI. Bar, 10 μm. (C) Immunoblots and phosphorylation profile of tau as detected with a panel of phosphorylation-sensitive antibodies. Lysates were prepared from stably transfected FLAG-tau (352 tau)-expressing cells. Immunoblots are shown for different phosphorylation-sensitive antibodies as indicated (top) and phosphorylation-insensitive Tau5 antibody (bottom). Relative immunoreactivity against individual phosphoepitopes was calculated from the total intensities of all tau-reactive bands per lane divided by Tau5 immunoreactivity. To plot a phosphorylation profile, the respective values for R406W tau were expressed relative to wt tau, which was set as 100%. Mean and range from two independent tau-expressing PC12 cell clones are shown (error bars). 25 μg of protein were loaded per lane. Note the decreased phosphorylation of mutant tau at several sites (T205, T212, and S396/404). The amount of endogenous tau was below the detection limit. Black lines indicate that intervening lines have been spliced out. (D) Immunoblots and relative immunoreactivity of 441 tau, as detected with a selection from the antibodies shown in C. Lysates were prepared from stably transfected Flag-tau (441 tau)-expressing cells. Phosphorylation was decreased at T205, T212, and at the PHF1-epitope, similar to 352 tau. Numbers to the sides of the gel blots indicate molecular mass standards in kilodaltons.

40–65%) as compared with wt tau, whereas other sites were not affected or only slightly affected (T181, S199, S214, and S262). We did not observe an increased phosphorylation of R406W tau at any of the sites analyzed. To determine whether the presence of the adult-specific exons affects phosphorylation, quantitative immunoblotting was also performed with lysates expressing the 441 tau isoforms using some of the phosphorylation-sensitive antibodies. Again, we did not observe a change with the Tau1 antibody, whereas phosphorylation was strongly decreased at T205, T212, and the PHF1 epitope (reductions of 40–80%; Fig. 1 D).
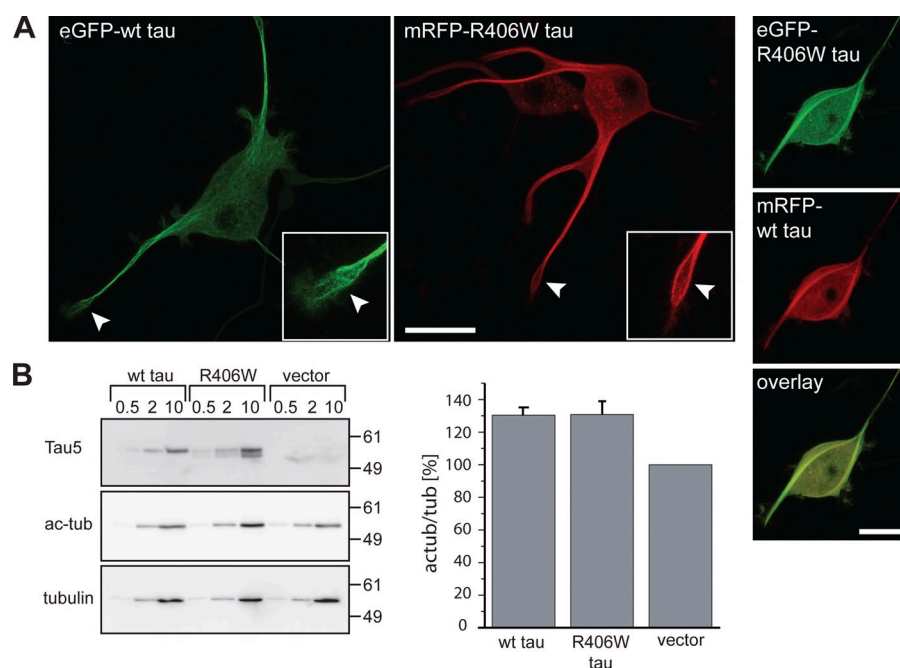
The data indicate that in PC12 cells, R406W tau is less phosphorylated at several disease-relevant sites than the wt protein.

The R406W mutation does not affect the interaction of tau with microtubules

During tauopathies, tau may change or lose its interaction with microtubules, which in turn may affect its distribution within neurons.

To assess this interaction for the R406W mutation, we transiently expressed fluorescently tagged tau constructs in

Figure 2. **Fluorescent-tagged wt and R406W tau interact similarly with microtubules.** (A) Fluorescence micrographs (left) and double fluorescence images (right) of detergent-extracted cells expressing the indicated tau constructs. The growth cone region is shown enlarged in the insets. Note the filamentous staining patterns in the growth cone regions (arrowheads) indicative of cytoskeletal association (left). Colocalization of wt tau and R406W tau suggests binding to the same subpopulation of microtubules (right). Bars, 20 μm. (B) Immunodetection of tau, acetylated tubulin (ac-tub), and total α-tubulin of lysates from tau-expressing and vector-control PC12 cell lines. Indicated amounts of protein were loaded per lane. Relative immunoreactivity of the ac-tub signal to total α-tubulin was calculated from the lanes where 10 μg of protein had been separated. Note the increased ratios of acetylated to total tubulin in human tau-expressing cells compared with control lines indicative of microtubule stabilization. No difference was observed between wt and R406W tau–expressing cells. Mean and range from two independent tau-expressing PC12 cell clones are shown (error bars). Experiments were performed with the 352 tau isoform. Numbers to the sides of the gel blots indicate molecular mass standards in kilodaltons.

PC12 cells, induced a neuronal phenotype by treatment with NGF, and performed a combined fixation–extraction protocol to visualize microtubule-associated tau protein (Fig. 2 A, left). We observed that wt tau and R406W tau exhibited a very similar filamentous staining pattern indicative of binding to microtubules. Both proteins were enriched in neurites and were also present in filamentous structures in growth cones (Fig. 2 A, left, arrowheads and insets). When wt tau and R406W tau were coexpressed in the same cell, no difference in the distribution was observed, as indicated by the yellow color in the overlay (Fig. 2 A, right). This suggests that both wt tau and R406W tau bind to the same microtubule subpopulations in NGF-differentiated PC12 cells.

It is known that binding of tau to microtubules results in increased microtubule stability, which is manifested by a higher ratio of acetylated/total tubulin (Piperno et al., 1987). To determine the degree of microtubule stabilization, lysates from cells that stably expressed FLAG-tagged wt tau and R406W tau were analyzed by immunoblotting and compared with control cells. Immunodetection used antibodies against tau, acetylated tubulin, and total α-tubulin (Fig. 2 B, left). Quantification revealed that wt tau and R406W tau expression led to an ∼30% increase in microtubule stability as compared with control cells (Fig. 2 B, right). No difference was observed between wt tau and R406W tau–expressing cells, again indicating that both proteins bind to the same extent to microtubules. Thus, the data indicate that despite its decreased phosphorylation, R406W tau does not enhance microtubule stabilization.

It is possible that wt tau and R406W tau bind in a different manner to microtubules, which could for example result in a displacement of mutant tau by wt tau from microtubules. To explore this hypothesis, we determined the effective diffusion coefficient (D_{eff}) of PAGFP-tau in neurites when coexpressed with mRFP-wt tau, mRFP-R406W tau, or the fluorescence tag alone.
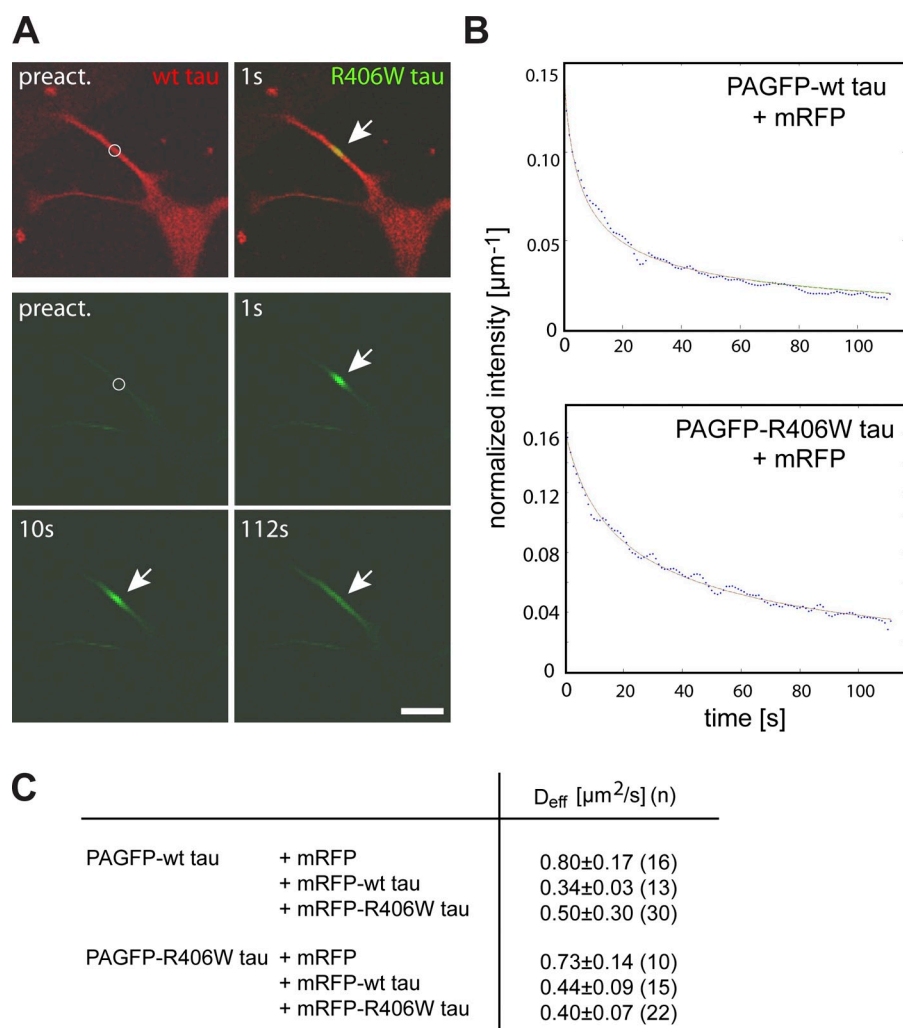
The distribution of focally activated PAGFP-tau (PAGFP*-tau) was recorded over time (Fig. 3 A). The fluorescence decay in the activated region was then plotted against the time, and D_{eff} was calculated as described previously using a modeling approach (Fig. 3 B; Weissmann et al., 2009). We did not find any difference in the D_{eff} of wt tau and R406W after coexpression with the fluorescence tag (mRFP) alone, which confirms that both proteins bind to microtubules to a similar extent (Fig. 3 C). The percentage of microtubule-bound tau can be calculated from $D_f/D_{eff} = 1 + K^*$, with K^* as the ratio of bound/free molecules (Sprague et al., 2004) and the diffusion coefficient of 3×PAGFP as a nonbinding control ($D_f = 6.3$ μm^2/s; Weissmann et al., 2009). These calculations indicated that the majority of wt tau and R406W tau (87% and 88%, respectively) was associated with microtubules in the neurites. Coexpression of mRFP-labeled tau constructs with PAGFP-tagged tau resulted in a decrease of D_{eff} by 40–60%, probably caused by increased molecular crowding on the microtubules. We did not observe an obvious difference in the D_{eff} of wt tau when coexpressed with the same construct or with R406W tau, or of R406W tau when coexpressed with the same construct or wt tau. This indicates that wt tau does not displace R406W tau from the surface of microtubules, or vice versa, and suggests that both proteins interact with microtubules in a very similar manner.

Collectively, the data indicate that the R406W mutation does not affect tau-dependent microtubule stabilization or the interaction of tau with microtubules in living cells.

R406W tau is deficient in binding to the neuronal membrane cortex and exhibits a reduced trapping in neurites

We have previously shown that tau interacts with the neural membrane cortex in a phosphorylation-dependent manner

A

B

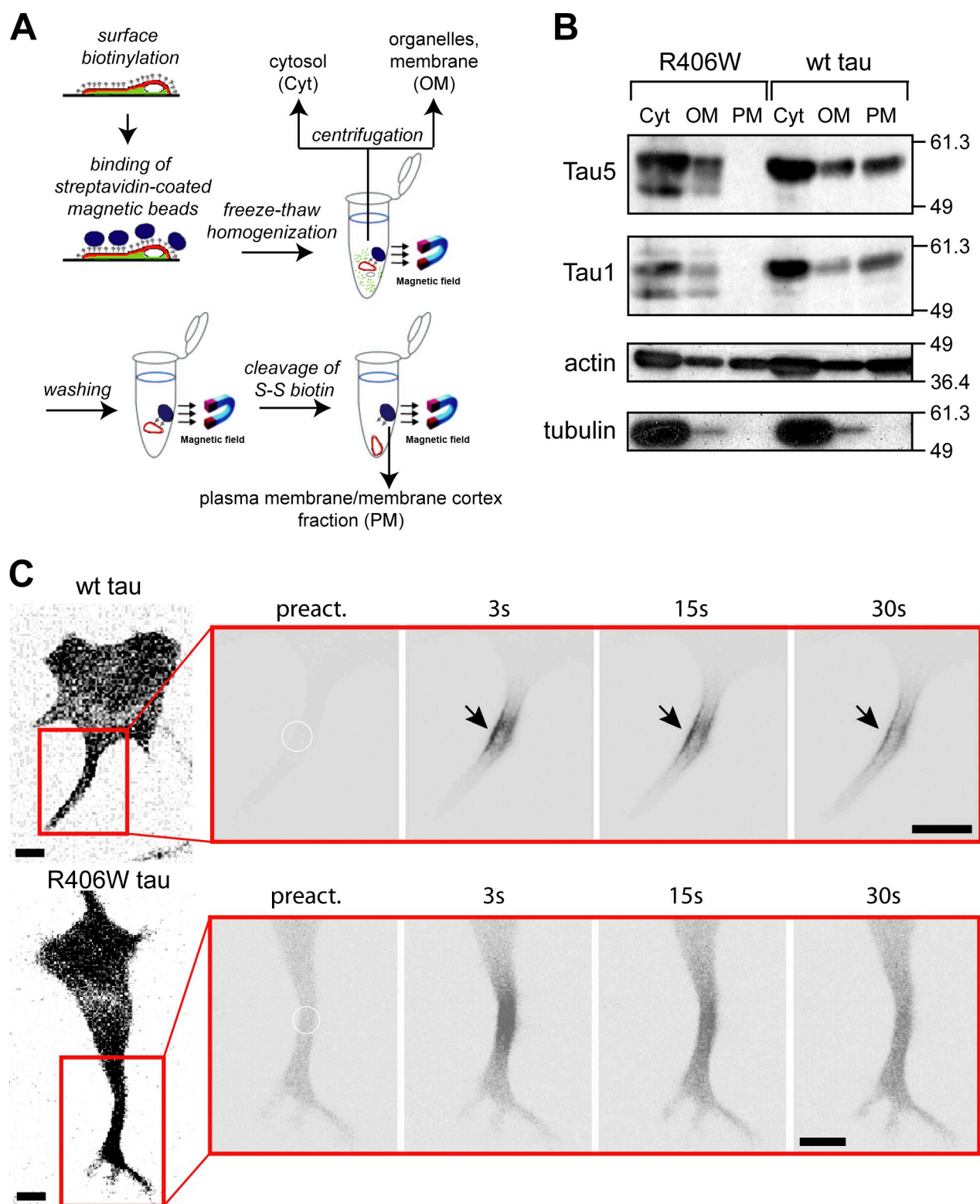Figure 3. **Wt and R406W tau exhibit same effective diffusion in the neuritic shaft.** (A) Live cell imaging of a PC12 cell coexpressing mRFP-tagged wt tau and PAGFP-tagged R406W tau after fluorescence photoactivation. The position of photoactivation is indicated by a circle in the preactivation images, and distribution between 1 and 112 s was determined. Fluorescence decay of PAGFP-R406W tau in the activated region as a result of diffusion is marked by the arrows. Bar, 20 µm. (B) Fits of representative decay plots to model diffusion of PAGFP-wt tau and R406W tau. Modeling was performed as described in Materials and methods. (C) Effective diffusion coefficients for PAGFP-tau in different combinations of coexpression. Stably transfected PAGFP-tau–expressing lines were transiently transfected with mRFP or mRFP-tagged constructs as indicated. Coexpression of tau constructs reduces the diffusion similarly for wt and R406W tau. Values are shown as mean ± SEM from fits of *n* processes. Experiments were performed with the 352 tau isoform.

C

		D_{eff} [µm²/s] (n)
PAGFP-wt tau	+ mRFP	0.80±0.17 (16)
	+ mRFP-wt tau	0.34±0.03 (13)
	+ mRFP-R406W tau	0.50±0.30 (30)
PAGFP-R406W tau	+ mRFP	0.73±0.14 (10)
	+ mRFP-wt tau	0.44±0.09 (15)
	+ mRFP-R406W tau	0.40±0.07 (22)

(Brandt et al., 1995; Maas et al., 2000). Tau's association with the membrane cortex may play an important role in the axonal localization of tau and may contribute to the trapping of tau in distal processes (Weissmann et al., 2009).

To determine whether the R406W mutation affects the association of tau with the membrane cortex, cell fractionations were used to enrich plasma membranes and proteins of the associated membrane cortex (PM fraction). The protocol is based on magnetic sphere separation of surface-biotinylated cells that were homogenized at mild conditions (Fig. 4 A). With this method, a PM fraction, which contains ∼30–35% of the total cellular actin, is obtained, indicating the presence of the actin-rich membrane cortex. This fraction is devoid of tubulin, which behaves as a soluble cytosolic protein under the conditions of fractionation (Fig. 4 B). In agreement with previous results (Maas et al., 2000), ∼20–30% of total wt tau was present in the PM fraction as detected with antibodies against total tau (Tau5) and a dephosphorylated tau epitope (Tau1). In contrast to wt tau, R406W tau was completely absent from the PM fraction. Quantification of the Tau5 blot revealed that the percentage of the tau signal in the organelle/membrane fraction was similar for R406W tau and wt tau (27% and 22%, respectively), whereas the percentage of cytosolic R406W tau was much higher (73% and 52% for

R406W tau and wt tau, respectively). This suggests that the nonplasma membrane-bound R406W tau is instead present in the cytosol. Thus, the data suggest that the R406W mutation abolishes tau's association with the membrane cortex and increases the amount of tau in the cytosolic fraction.

To determine whether the difference in membrane binding can also be visualized by fluorescence microscopy, we followed tau distribution after focal activation of tau. In fact, PAGFP*-wt tau showed a clear enrichment at the periphery, which suggests its membrane association, whereas PAGFP*-R406W tau exhibited a uniform distribution within the process (Fig. 4 C). To determine whether the difference in membrane binding affects trapping of tau in neurites, we photoactivated wt tau and R406W tau in the tip of a neurite and followed its distribution over time. It was evident from the color-coded plots of 2D intensity functions that PAGFP*-R406W dissipated faster from the activation spot than PAGFP*-wt tau (Fig. 5 A). For quantification of the extent of trapping, the fraction of tau in the activated spot was compared with total tau (I_t/I_{tot}) at different time points after activation. We observed that I_t/I_{tot} was significantly higher for wt tau as compared with R406W tau (Fig. 5 B). This indicates a preferential trapping of wt tau in agreement with its ability to interact with the plasma membrane. We determined the effective

Figure 4. **R406W tau is deficient in binding to the neural plasma membrane.** (A) Schematic representation of the plasma membrane fractionation assay to analyze tau's interaction with the neural membrane cortex. (B) Immunoblot showing the distribution of FLAG-tagged tau, actin, and tubulin in the cytosolic (Cyt), organelles/membrane (OM), and plasma membrane/membrane cortex (PM) fractions. Note the complete absence of R406W tau mutant in the PM fraction, whereas a major amount of wt tau is PM-associated. Numbers to the sides of the gel blots indicate molecular mass standards in kilodaltons. (C) Time-lapse microscopic images of processes from PC12 cells expressing PAGFP-tagged tau constructs after photoactivation. A close-up of the processes (red box) is shown and the position of photoactivation is indicated by a circle. Note the enrichment of wt tau close to the plasma membrane (arrows), whereas R406W tau shows a uniform distribution. Experiments were performed with the 352 tau isoform. Bar, 10 µm.

diffusion constants for wt and R406W tau after activation in the tip by taking into account that diffusion is restricted to one direction. D_{eff} in the tip was less than half for wt tau compared with R406W tau (Fig. 5 C) and compared with the diffusion of tau in the shaft (see Fig. 3). The data suggest that tau's membrane association causes retention of tau in the tip of neurites, which is compromised by the R406W mutation.
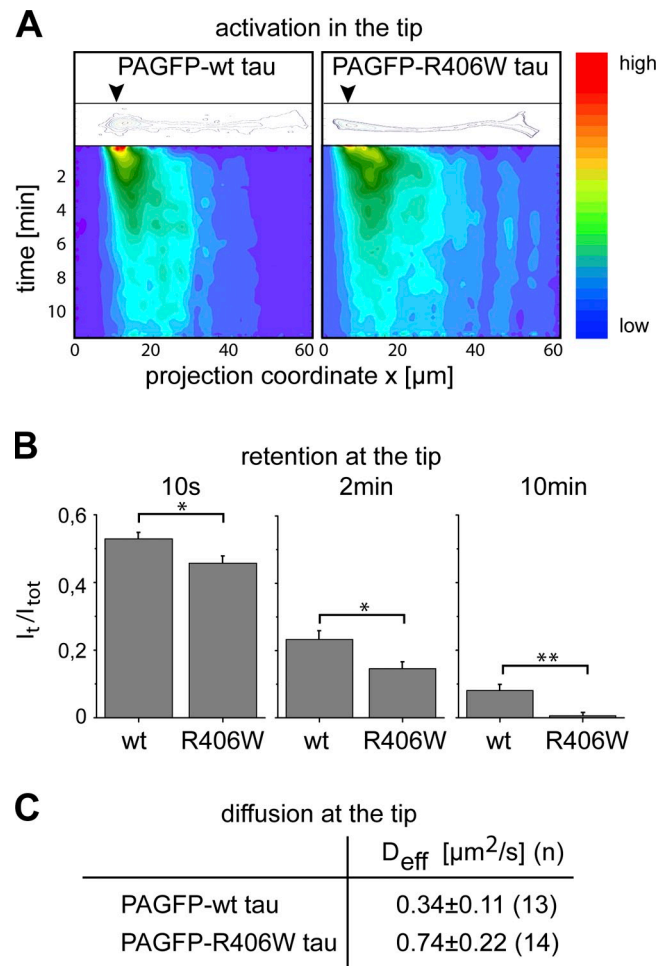
The R406W mutation causes fluctuations during process outgrowth

The data presented indicate that wt tau and R406W tau differ in their ability to interact with membranes in the processes of neural cells. Consequently, the loss of membrane interaction as a result of the R406W mutation could also affect neurite extension.

To test whether tau's membrane interaction influences process extension in differentiating PC12 cells, process growth was followed by live cell imaging of NGF-treated PC12 cells, which stably expressed EGFP-tagged wt tau or R406W tau. We observed that processes of cells expressing wt tau appeared to continuously extend their length with time in culture (Fig. 6 A, top; and Fig. 6 B, left). In contrast, processes from R406W tau–expressing cells showed large fluctuations between elongating and shrinking states (Fig. 6 A, bottom; and Fig. 6 B, right). Quantification confirmed that R406W tau–expressing cells exhibited larger length changes during process growth compared with wt tau–expressing or EGFP-expressing control cells (Fig. 6 C). The total length of the processes did not differ between cells expressing the two tau constructs, as determined from population analysis after 6 d of NGF treatment (Fig. 6 D). The data indicate that the R406W mutation induces larger fluctuations in elongation rates, which suggests that tau's membrane interaction stabilizes process growth.

The plasma membrane–associated protein annexin A2 (AnxA2) functionally interacts with tau to mediate trapping in neurites
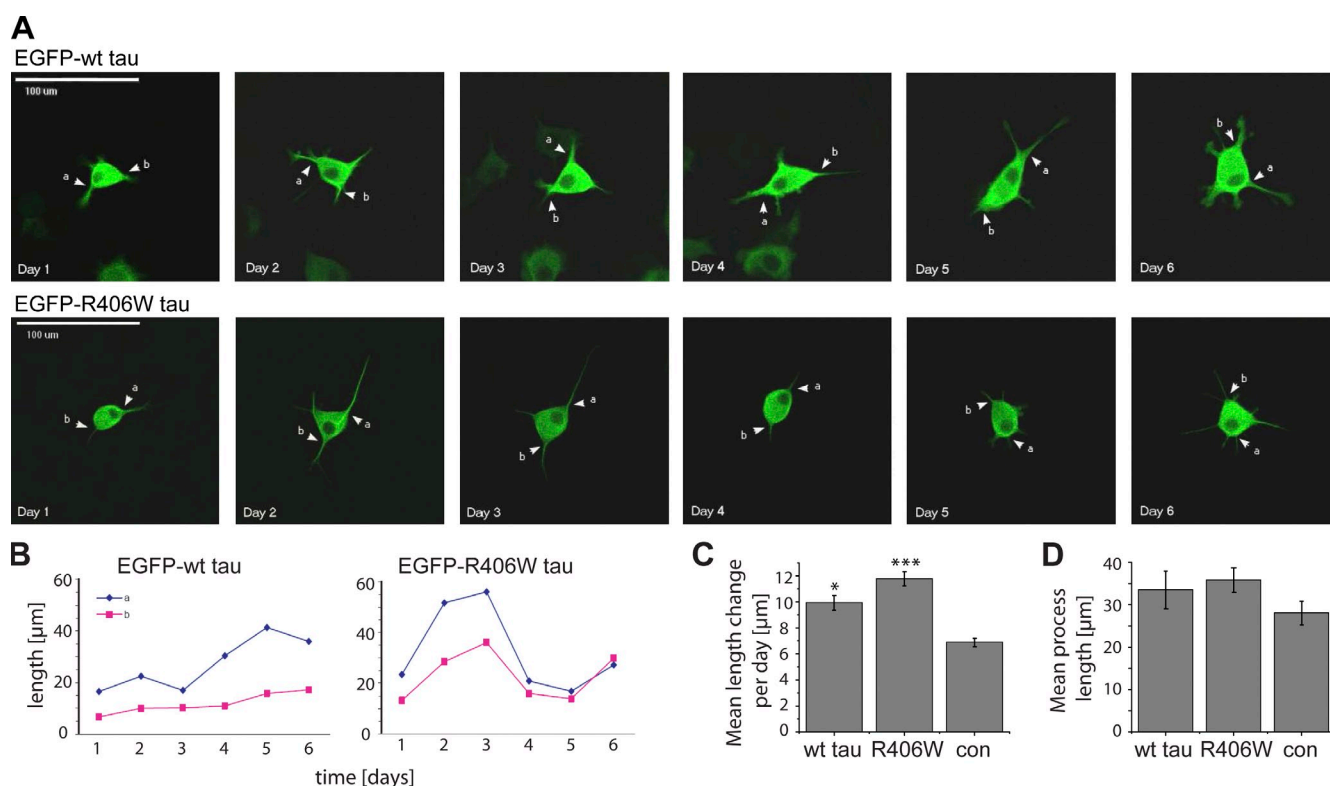
Because the wt protein associates with the membrane cortex, in contrast to R406W tau, we performed TAP tag MS of tau-transfected neural cells to identify membranous or membrane-associated proteins as potential tau interaction partners. To solubilize the membrane, lysates were prepared at low detergent concentrations (0.15% NP-40). With this approach, the calcium-regulated membrane and microfilament-interacting protein AnxA2 was identified as a prominent component of a tau-containing complex (Fig. 7 A). To test for a direct interaction between tau and AnxA2, we performed yeast two-hybrid experiments with human wt tau, R406W tau, and human AnxA2. None of the tested combinations displayed any interaction (unpublished data). Thus, either tau and AnxA2 do not directly interact, or the interaction may not occur within the yeast nuclear environment (e.g., because of the absence of suitable membrane components or an inappropriate Ca^{2+} concentration). To test for interaction of AnxA2 and tau in PC12 cells, cellular lysates were prepared and PAGFP-tau was precipitated using a GFP-trap in the presence of NP-40. We did not detect endogenous AnxA2 coprecipitating with human tau when the experiments were performed in the absence of Ca^{2+} (unpublished data).

Figure 5. **R406W tau exhibits reduced trapping in the tip of neurites compared with wt tau.** (A) Contour and color-coded plots of 2D intensity functions after photoactivation in the tip of representative processes expressing PAGFP wt and R406W tau. Position of activation is indicated by black arrowheads in the contour plot. Fluorescence intensity is color-coded from blue to red as indicated on the right. Note that the dissipation of fluorescence in the activated region occurs faster with R406W tau compared with wt tau. (B) Quantification of retention after focal activation of wt and R406W tau in the tip of neurites. Immobile fractions at different time points after activation (I_t/I_{tot}) show decreased retention of R406W compared with wt tau. Values are shown as mean ± SEM (error bars). **, P < 0.01; *, P < 0.05 (n = 12–21). (C) Effective diffusion coefficients of tau after photoactivation at the tip of processes in PC12 cells stably expressing PAGFP wt tau or R406W tau. Values are shown as mean ± SEM with fits from n cells. Note the decreased D_{eff} value corresponding to the increased retention of wt tau compared with R406W tau. Experiments were performed with the 352 tau isoform.

Unfortunately, the presence of Ca^{2+} resulted in the precipitation of AnxA2 even at control conditions (PAGFP alone; unpublished data), probably because of the formation of unspecific complexes in the presence of neural membrane components. To overcome this limitation, we coexpressed human tau with GFP-tagged human AnxA2 in the heterologous yeast system. The proteins were clearly produced and present in crude extracts (Fig. 7 B, input). In pull-down assays in the presence of Ca^{2+}, between 25 and 40% wt tau coprecipitated with AnxA2, whereas R406W tau remained completely in the supernatant (Fig. 7 B, top). Coprecipitation occurred with both the 352 and

Figure 6. The R406W mutation induces higher fluctuations during process growth. (A) Live imaging of PC12 cells stably expressing EGFP-tagged wt tau and R406W tau. Fluorescence micrographs of the same cell at different times after induction of differentiation with NGF are shown. Two representative processes per cell are followed over time and are indicated by arrowheads. Bar, 100 µm. (B) Plot of the lengths of the representative processes indicated in A over time. Note that the processes of the R406W tau–expressing cell showed large fluctuations in lengths over time. (C) Quantification of mean length change per day for tau-expressing cells compared with an EGFP-expressing control (con). Results are shown as mean ± SEM (error bars). ***, P < 0.001; *, P < 0.05 compared with the EGFP-expressing control ($n = 52$–81 processes). Two independent clonal lines were used per construct. (D) Mean length of processes after 6 d of NGF treatment as determined by population analysis. 23–31 of processes were measured for the respective cell lines. Mean process lengths ± SEM are given (error bars). Note that the overall process length is similar for tau-expressing cells. Experiments were performed with the 352 tau isoform.

the 441 wt tau isoform, indicating that the additional exons were not required for the interaction with AnxA2. In control experiments where GFP was coexpressed with the tau constructs, neither 352 nor 441 tau precipitated. Thus, the data indicate that in a heterologous yeast system, AnxA2 and tau specifically interact.

To test whether tau and annexin could also interact in neural cells, we performed colocalization experiments in differentiated PC12 cells and primary cortical cultures. Endogenous AnxA2 was present in the cell body and in processes, where it showed enrichment in distal tips (Fig. 8 A). Transfected tau was also present in the cell body, the neurites, and the tip of processes. In growth cones, we observed colocalization of tau and AnxA2 in filamentous structures (Fig. 8 A, insets), which is consistent with a tau–annexin interaction in this region. To test for interaction with cytoskeletal structures, we performed a combined fixation–extraction protocol. We observed that a significant amount of AnxA2 was retained together with tau in the cell body, neurites of differentiated PC12 cells (Fig. 8 B), and axons of primary cortical cultures (Fig. 8 C), confirming that tau and AnxA2 are present in the same compartment and associate with cytoskeletal structures.
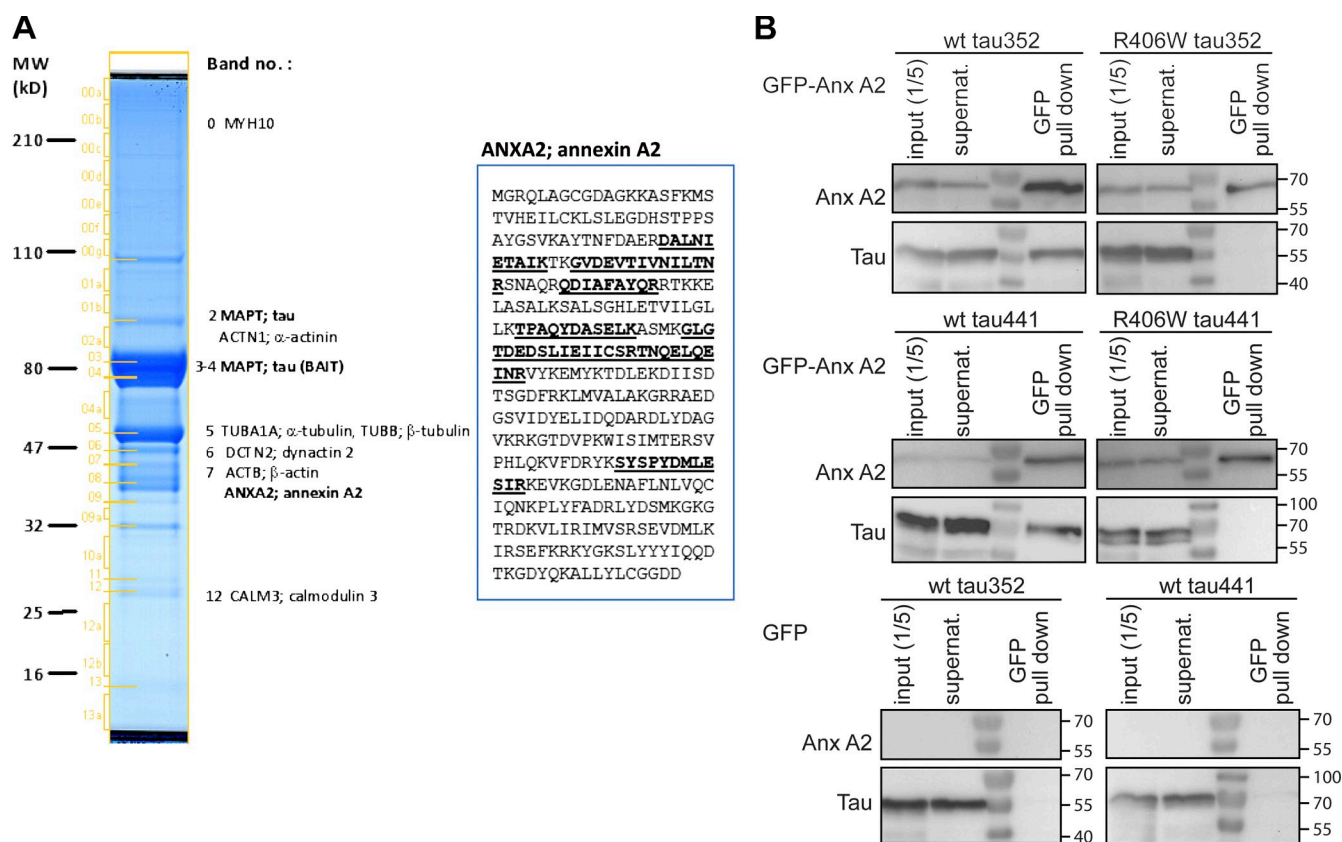
To test for a functional interaction between tau and annexin in neurites, we knocked down AnxA2 in PC12 cells by small hairpin RNA (shRNA). For these experiments, cells that stably

expressed wt tau or R406W tau were infected with lentivirus encoding AnxA2 shRNA or a control shRNA. Infected cells were selected with puromycin. Western blot analysis showed that the amount of AnxA2 strongly decreased to $21.7 \pm 5.5\%$ ($n = 4$) with AnxA2 shRNA, whereas only minor changes were observed when the cells were treated with the control shRNA (Fig. 9 A). Consequently, a strong reduction of annexin staining was also observed by immunocytochemistry (Fig. 9 B). It should be noted that tau levels were approximately twice as high in cells that have been treated with AnxA2 shRNA compared with untreated cells. We also observed that treatment with the control shRNA increased the amount of tau to a similar extent, which indicates that the changes in tau expression are related to the puromycin treatment during the selection and not to AnxA2 knockdown.

The effect of AnxA2 knockdown on tau trapping was then analyzed after photoactivation of tau in the tip of neurites. We observed that the difference in the retention of wt tau and R406W tau was abolished after annexin knockdown (Fig. 9 C). In agreement, D_{eff} in the tip was much lower for wt tau compared with R406W tau after infection with the control shRNA, whereas it was similar in AnxA2 shRNA–treated cells (Fig. 9 C, right).

Because it is known that binding of AnxA2 to membranes requires calcium (Gerke and Moss, 2002; Gerke et al., 2005), we treated cells expressing wt tau or R406W tau (in the absence

A

MW (kD)

Band no.:

0 MYH10

210 —

110 —

80 —

47 —

32 —

25 —

16 —

2 MAPT; tau
   ACTN1; α-actinin

3-4 MAPT; tau (BAIT)

5 TUBA1A; α-tubulin, TUBB; β-tubulin
6 DCTN2; dynactin 2
7 ACTB; β-actin
   ANXA2; annexin A2

12 CALM3; calmodulin 3

ANXA2; annexin A2

MGRQLAGCGDAGKKASFKMS
TVHEILCKLSLEGDHSTPPS
AYGSVKAYTNFDAER**DALNI
ETAIK**TK**GVDEVTIVNILTN
R**SNAQR**QDIAFAYQR**RTKKE
LASALKSALSGHLETVILGL
LK**TPAQYDASELK**ASMK**GLG
TDEDSLIEIICSRTNQELQE
INR**VYKEMYKTDLEKDIISD
TSGDFRKLMVALAKGRRAED
GSVIDYELIDQDARDLYDAG
VKRKGTDVPKWISIMTERSV
PHLQKVFDRYK**SYSPYDMLE
SIR**KEVKGDLENAFLNLVQC
IQNKPLYFADRLYDSMKGKG
TRDKVLIRIMVSRSEVDMLK
IRSEFKRKYGKSLYYYIQQD
TKGDYQKALLYLCGGDD

B

GFP-Anx A2 — wt tau352 / R406W tau352
Anx A2 / Tau — 70, 55, 40

GFP-Anx A2 — wt tau441 / R406W tau441
Anx A2 / Tau — 70, 55, 100, 70

GFP — wt tau352 / wt tau441
Anx A2 / Tau — 70, 55, 40, 100

Figure 7.   **Identification of annexinA2 as a putative tau interaction partner.** (A) TAP of tau protein. Amino-terminally TAP-tagged 441 tau was purified from SKNBE2 cells, separated by SDS-PAGE, and stained with colloidal Coomassie. The overexpressed tau protein is clearly visible at an apparent molecular mass of 70–80 kD. Copurifying proteins identified by LC-MS/MS are labeled. The sequence coverage for the AnxA2 protein sequence was 23% (indicated by marking sequenced peptides underlined and in boldface). (B) Pull-down of GFP-tagged Anx A2 fusion constructs in yeast. Wt tau coprecipitated after pull-down of GFP–Anx A2. No coprecipitation of R406W tau was observed. In control experiments (pull-down of GFP), wt tau did not coprecipitate. Numbers to the sides of the gel blots indicate molecular mass standards in kilodaltons.
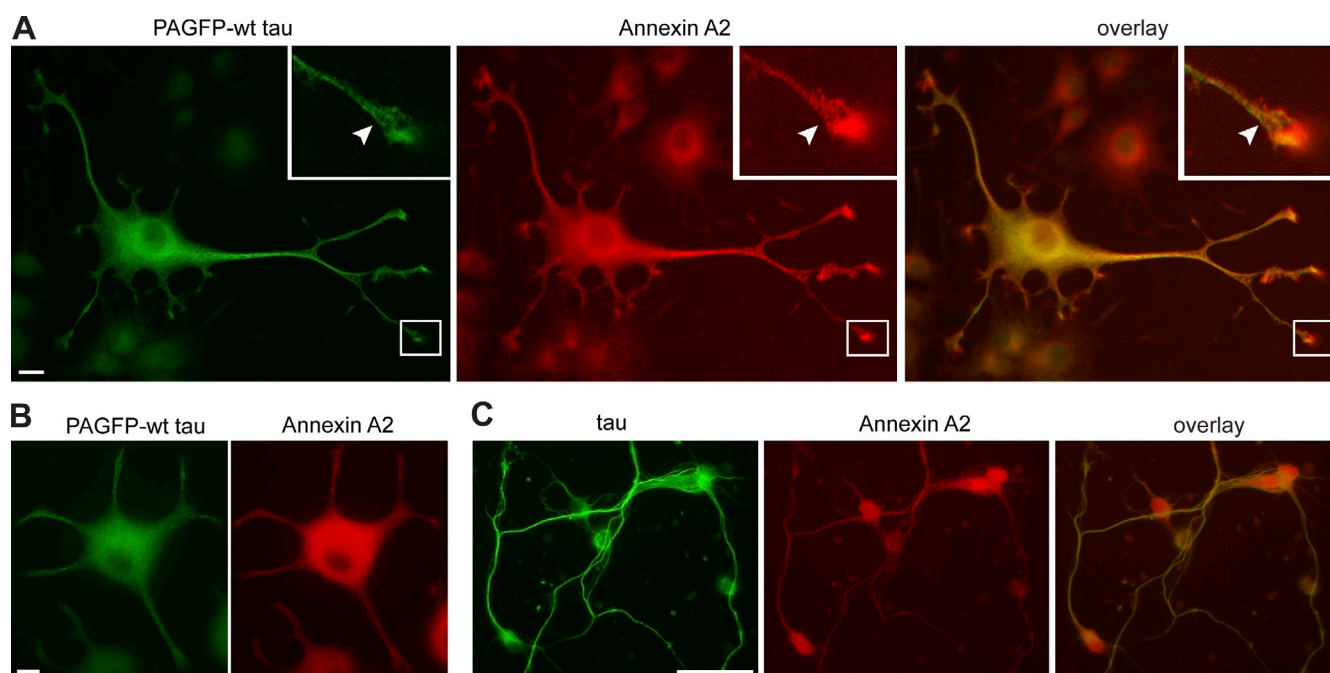
of shRNA) with the cell-permeable calcium chelator BAPTA/AM to interfere with the annexin–membrane interaction. Also, after BAPTA treatment, the difference in the retention of wt tau and R406W tau was abolished (Fig. 9 D), which again suggests that tau trapping is caused by an interaction with AnxA2 at the membrane.

If AnxA2 causes retention of wt tau due to a functional interaction in the tip of processes, it may be expected that, in turn, wt tau expression reduces the mobility of AnxA2 in growth cones. To test this hypothesis, we prepared an AnxA2–PAGFP fusion construct and expressed it in PC12 cells. An immunoblot of cellular lysates confirmed that the full-length construct was expressed in infected cells in addition to endogenous annexin (Fig. 10 A). We observed that AnxA2–PAGFP was distributed in the cytosol and the processes and showed an enrichment at the tip of neurites similar to endogenous AnxA2 (Fig. 10 B, compare with Fig. 8 A). Wt tau colocalized with AnxA2–PAGFP at the tip while R406W tau was absent. To test whether tau expression affects the mobility of AnxA2, we performed fluorescence decay after photoactivation experiments where AnxA2–PAGFP was activated at the tip of the processes and its dissipation followed over time. We observed that wt tau expression caused an increased retention of AnxA2–PAGFP* in the tip compared with R406W tau–expressing or untransfected control cells (Fig. 10 C).

Collectively, the data indicate that wt tau but not R406W tau functionally interact with AnxA2 in neural growth cones and suggest that this interaction regulates the distribution of both proteins.

Discussion

We have shown that the R406W FTD tau mutation abolishes the ability of tau to interact with the neural membrane cortex and reduces trapping of tau in the tip of neuron-like processes. In contrast, microtubule-related features such as the activity to stabilize microtubules or the extent and dynamics of microtubule binding in neuronal processes were unaffected by the mutation. Previously, it had been shown that some FTDP-17 mutations compromised tau's ability to affect microtubule dynamics, whereas the R406W mutation did not alter microtubule-related activities (Bunker et al., 2006) and was indistinguishable in the colocalization pattern with microtubules (DeTure et al., 2000). This is consistent with the idea that at least some FTDP-17 mutations affect other activities of tau rather than binding to microtubules. It will be interesting to determine whether other tau mutations that have been frequently observed in FTDP-17 cases such as G272V and P301L also influence tau's interaction with annexin.
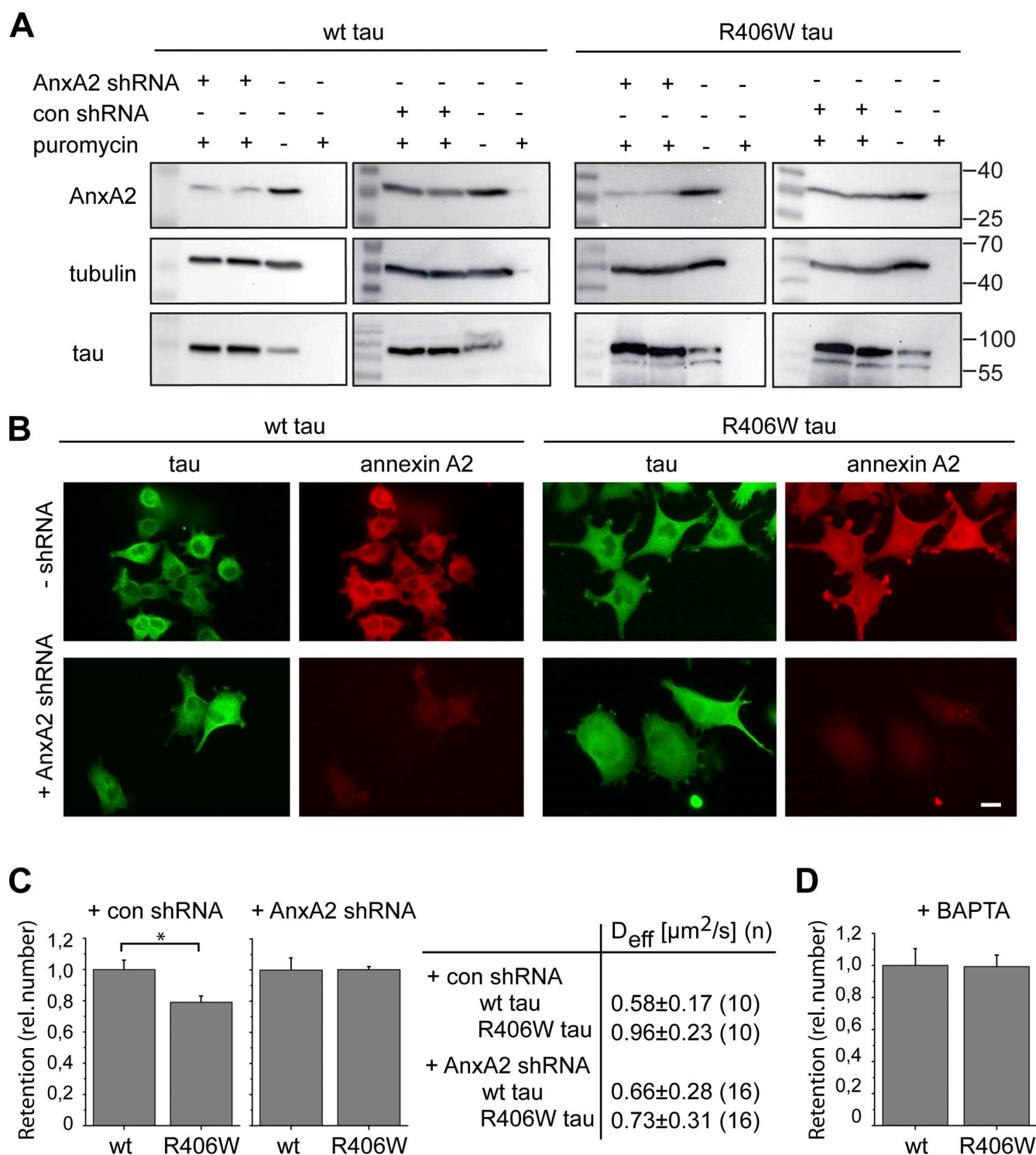
Figure 8. **Distribution of tau and AnxA2 in PC12 cells and primary cortical neurons.** (A) Fluorescence micrographs of neuronally differentiated PC12 cells stably expressing PAGFP wt tau. Cells were fixed with paraformaldehyde and stained against GFP and endogenous AnxA2. The growth cone region is shown enlarged in the insets. Note the enrichment of AnxA2 at the tip of processes and colocalization of tau and AnxA2 in filamentous structures of the growth cone (arrowheads). (B and C) Fluorescence micrographs of PC12 cells stably expressing PAGFP wt tau (B) and primary cortical neurons (C) after a combined detergent extraction–fixation protocol to reveal cytoskeletal association. PC12 cells were stained against GFP and endogenous AnxA2, and cortical neurons were stained against endogenous tau and AnxA2. Note that a significant amount of AnxA2 is retained together with tau in the cell body and neurites of PC12 cells, as well as the axons of primary neurons. Experiments were performed with the 352 tau isoform. Bars: (A and B) 10 µm; (C) 50 µm.

The R406W mutation reduced rather than increased phosphorylation at several positions, including the PHF1 epitope (S396/S404), T212, and T205. Decreased phosphorylation of R406W tau at several sites has also been reported earlier in different cellular systems (Dayanandan et al., 1999; Matsumura et al., 1999; Vogelsberg-Ragaglia et al., 2000; DeTure et al., 2002; Tackenberg and Brandt, 2009). Among others, all of these sites can be phosphorylated in vitro by the kinases Cdk5 and GSK3β, both of which have been implicated as having a role in AD (Cruz and Tsai, 2004; Hooper et al., 2008). The data presented here also indicate that phosphorylation at these positions does not affect tau's ability to stabilize microtubules. This is in agreement with the finding that the extent of phosphorylation at Ser262, which is located within the microtubule-binding region and known to critically affect tau's microtubule interaction (Biernat et al., 1993), was not significantly changed in the R406W variant. However, it is possible that the changes in the phosphorylation profile that are induced by the R406W mutation induce more subtle changes with respect to tau's microtubule-related activities.

On first view, it appears surprising that a mutation in tau's carboxy-terminal region selectively affects a feature that is known to be mediated by the opposite side of the molecule, the amino-terminal projection domain of tau. However, it has been shown previously that tau can adopt a "paperclip" conformation, in which the amino- and carboxy-terminal domains approach each other (Jeganathan et al., 2006). Furthermore, MS analysis of the phosphorylation pattern suggested that the
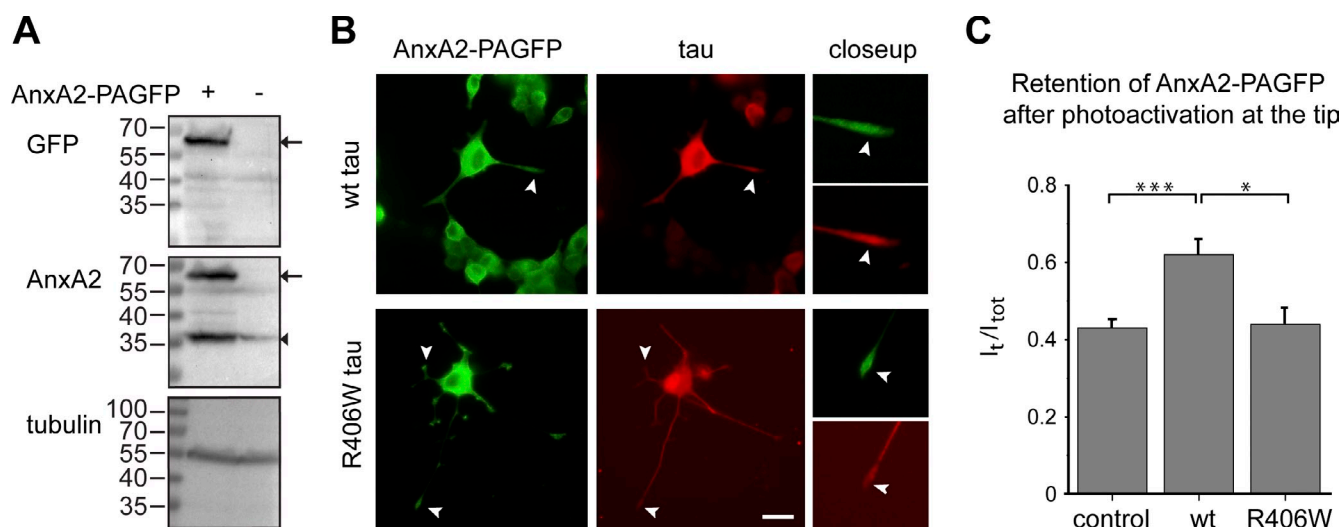
R406W mutation exerts long-range conformational effects on the structure of tau (Connell et al., 2001), which could explain an effect of the carboxy-terminal mutation on the amino-terminal domain. This is also consistent with the reduced phosphorylation of T205 and T212 in R406W tau compared with wt tau, residues that are both located in the amino-terminal half of the protein. Previously, we have observed similar and selective long-range effects when we analyzed the influence of phosphorylation on tau's ability to interact with the membrane cortex. We found that pseudophosphorylation in tau's carboxy terminus abolished tau's interaction with the membrane cortex, whereas tau's ability to promote microtubule assembly was unchanged (Eidenmüller et al., 2001).

What is the functional role of tau's interaction with the membrane? We previously demonstrated that overexpression of tau's amino terminus inhibits process outgrowth in cells (Brandt et al., 1995), and suggested that tau's membrane interaction supports process formation that is competitively suppressed by the amino-terminal fragment. Consistent with this hypothesis, we have found here that R406W tau–expressing cells showed higher fluctuations in process extension compared with wt tau, which may suggest that tau's membrane interaction supports stable process growth, presumably by bridging the growing microtubules to the membrane cortex in the growth cone. Our data suggest that this bridging is mediated by AnxA2 (see the following paragraph). It has been reported that AnxA2 is up-regulated during NGF-induced differentiation of PC12 cells (Schlaepfer and Haigler, 1990; Fox et al., 1991), which parallels

Figure 9. **Annexin A2 is required for trapping of wt tau in the tip of neurites.** (A) Immunoblots demonstrating shRNA-mediated knockdown of AnxA2 in PC12 cells. PC12 cells stably expressing PAGFP wt tau or R406W tau were infected with lentiviral particles coding for AnxA2 shRNA (AnxA2 shRNA) or a control shRNA (con shRNA). Infected cells were selected with puromycin as described in Materials and methods. Annexin A2 protein is reduced by ~80% in AnxA2 shRNA-treated cells. (B) Immunofluorescence images of PC12 cells stably expressing PAGFP wt tau and R406W tau with or without shRNA-mediated annexin knockdown. Staining was against AnxA2 and the GFP tag. After knockdown, AnxA2 is hardly detectable by immunofluorescence. Bar, 10 μm. (C) Retention of wt tau and R406W tau in the tip of processes after treatment with control shRNA and after shRNA-mediated AnxA2 knockdown. Immobile fractions after activation (I_t/I_{tot}) were determined after 10 s and expressed relative to wt tau. Values are shown as mean ± SEM (error bars); *, P < 0.05 (n = 10–16). Effective diffusion coefficients of the respective experiments are shown in the table. Values are shown as mean ± SEM with fits from n cells. Note that annexin knockdown abolished the difference in retention and D_{eff} values between wt tau and R406W tau. (D) Retention of wt tau and R406W tau in the tip of processes in the presence of the calcium chelator BAPTA/AM (BAPTA). Immobile fractions were determined as described in C. Note that the different retention of wt tau and R406W tau is abolished in the presence of BAPTA. Values are shown as mean ± SEM (error bars; n = 11–16). Experiments were performed with the 352 tau isoform.

Figure 10. **Tau expression reduces the mobility of AnxA2 in growth cones.** (A) Immunoblot showing the expression of PAGFP-tagged AnxA2 at the expected size (arrows). Endogenous annexin is indicated by the arrowhead. Tubulin is stained as loading control. (B) Fluorescence micrographs of PC12 cells stably expressing FLAG-tagged wt tau or R406W tau after infection with a lentivirus encoding AnxA2–PAGFP. Cells were fixed with paraformaldehyde and stained with antibodies against GFP (for AnxA2–PAGFP) and the FLAG-epitope (for tau). Close-ups of the tips of processes are shown on the right. Note that AnxA2–PAGFP showed an enrichment at the tip of neurites similar to endogenous AnxA2. Wt tau colocalized with AnxA2–PAGFP at the tip while R406W tau was absent (arrowheads). Bar, 10 µm. (C) Retention of AnxA2–PAGFP at the tip of neuronally differentiated PC12 cells stably expressing FLAG-tagged wt tau, R406W tau, or control cells. Note the increased retention of AnxA2–PAGFP* in wt tau, but not in R406W tau–expressing cells or control cells. Values are shown as mean ± SEM (error bars). ***, P < 0.001; *, P < 0.05 (n = 6–27). Experiments were performed with the 352 tau isoform.

the increased expression of tau (Drubin et al., 1988). This would be consistent with an involvement of both proteins in regulating neurite outgrowth (Fox et al., 1991; Jacovina et al., 2001). Very recently, it has been reported that tau affects neurite initiation without requirement for microtubule binding (Leugers and Lee, 2010). It is conceivable that tau's association with the membrane cortex is also involved in this activity.

Several lines of evidence reported here support the finding that tau interacts with AnxA2. (a) Annexin A2 was identified as an interacting protein using a TAP tag approach with tau as a bait. (b) Tau coprecipitated with AnxA2 in a heterologous yeast expression system. (c) Tau and AnxA2 colocalized in neuronally differentiated cells, and we observed colocalization of tau and AnxA2 in filamentous structures in the growth cones. (d) shRNA-mediated AnxA2 knockdown abolished trapping of tau in the tip of neurites. (e) Chelation of Ca^{2+} ions by treatment with BAPTA/AM, which is known to remove annexin from the plasma membrane, increases the mobility of tau in the tip of neurites. (f) Expression of tau increases the retention of AnxA2 in distal processes. Annexins are a multigene family of calcium-regulated membrane-binding proteins, which are expressed in most eukaryotic cell types and species (Gerke and Moss, 2002). In vertebrates, 12 subfamilies are expressed, termed A1–11 and A13 (Morgan and Fernández, 1997). The annexins share a core domain, which serves as a general membrane-binding module consisting of four α-helical annexin repeats and an amino-terminal head region of various lengths, which extends into the cytosol (Rescher and Gerke, 2004). Annexin A2 is mainly localized at the plasma membrane and the N-terminal domain modulates its membrane binding activity (Gerke and Moss, 2002). Plasma membrane binding is reversible and chelation of calcium results in liberation of AnxA2 from the membrane. Thus, the localization and distribution of AnxA2 may be

determined by differential intracellular calcium concentrations in the cell (Gerke and Moss, 1997). Ca^{2+}-regulated membrane binding of AnxA2 could also provide a mechanism to localize tau in an activity-dependent manner to the presynaptic region, thus regulating microtubule dynamics in parallel to the firing of a synapse.

Mice lacking AnxA2 show no obvious phenotypic change. Therefore, it has been proposed that other annexins can compensate for a functional loss of AnxA2 in a knockout scenario (Rescher and Gerke, 2004). Thus, transient down-regulation by RNA interference or expression of dominant interfering mutants may be more informative to analyze AnxA2-mediated activities. In fact, we observed that lentiviral shRNA administration caused a transient decrease of AnxA2 in cells and affected the trapping of tau in neuronal processes. In contrast, long-term expression of shRNA did not result in a decrease of AnxA2 protein, probably because of compensating mechanisms (unpublished data).

Our observation that the R406W mutation reduces trapping of tau in the distal neurite, which is probably caused by its decreased interaction with AnxA2, could be relevant in a neurodegenerative scenario. Decreased binding of R406W tau could result in a reduced stability of the presynapse and a distribution of tau R406W, which is less confined to the distal process. In this context, it appears remarkable that both Aβ-mediated hyperphosphorylation of tau in an AD scenario and the R406W mutation converge with respect to a loss of function of tau to interact with the plasma membrane. This could provide an explanation as to why the R406W tau mutation produces a phenotype that is clinically closely related to AD. Interestingly, in pathological conditions including seizures and AD, AnxA2 expression is increased (Eberhard et al., 1994). This could point to a compensatory mechanism of affected neurons in an attempt to rescue tau's membrane interaction in such patients.

Materials and methods

Materials and antibodies

Chemicals were obtained from Sigma-Aldrich, cell culture media and supplements were obtained from Sigma-Aldrich and Invitrogen, and culture flasks, plates, and dishes from were obtained from Thermo Fisher Scientific, unless stated otherwise. The following antibodies were used. Phosphorylation-independent human tau antibodies: Tau-5 (mouse; BD) and anti-tau (rabbit; Synaptic Systems GmbH). Phosphorylation-dependent tau antibodies: AT270 (Thr-181, mouse; Pierce), pT205 (Thr-205, rabbit; Invitrogen), pT212 (Thr-212, rabbit; Invitrogen), p214 (Ser-214, rabbit; Invitrogen), pS262 (Ser-262, rabbit; Invitrogen), PHF1 (mouse; a generous gift of P. Davies, Albert Einstein College of Medicine, Bronx, NY), and Tau-1 (mouse; a generous gift of L. Binder, Northwestern University, Chicago, IL). Also used were anti-GFP (rabbit; Invitrogen), anti-FLAG (M5), anti-tubulin (mouse, DM1A; rat, YL1/2), anti-acetylated tubulin (mouse; 6-11B-1), anti-actin (mouse, JLA20; EMD) and anti-AnxA2 (mouse, annexin II [H-5], Santa Cruz Biotechnology; mouse, HH7 [Thiel et al., 1992]). As secondary antibodies, peroxidase-, Cy3-, and Alexa Fluor 488–conjugated anti–mouse and anti–rabbit antibodies (Jackson ImmunoResearch Laboratories, Inc.) were used.

Construction of expression vectors, transfections, and lentiviral infections

Eukaryotic expression plasmids for fetal (352 aa) or adult (441 aa) human tau with amino-terminally fused FLAG, mRFP, EGFP, and PAGFP tags were constructed in pRc/cytomegalovirus (CMV)-based expression vectors (Invitrogen) containing a CMV promoter and kanamycin and neomycin resistance genes. PAGFP was constructed from EGFP by changing the codons L64F, T65S, V163A, and T203H by site-directed mutagenesis with primers as described previously (Patterson and Lippincott-Schwartz, 2002). The vector pSETbmRFP was provided by R.Y. Tsien (University of California, San Diego, La Jolla, CA). To produce R406W tau constructs, R406 was mutated to W by site-directed mutagenesis of the respective codon. Annexin A2 amino-terminally fused to PAGFP was cloned into the lentiviral vector L26FSy(1.1)GW (provided by P. Osten, Northwestern University, Chicago, IL), which contains the neuron-specific promoter Synapsin I (Dittgen et al., 2004). Sequences that were introduced by PCR were verified by DNA sequencing.

Transfections of PC12 cells were performed with Lipofectamine 2000 (Invitrogen) essentially as described previously (Fath et al., 2002). For generation of stable lines, individual clones were selected in the presence of 500 µg/ml Geneticin, then picked and propagated in serum-DME supplemented with 250 µg/ml Geneticin on collagen-coated culture dishes as described previously (Brandt et al., 1995). For each construct, several independent clonal lines were selected that expressed comparable levels of the protein.

For production of lentivirus, human embryonic kidney cells 293FT (Invitrogen) were transfected with the expression vector and two helper plasmids using TransIT-293 transfection reagent (Mirus Bio LLC). Viral particles from the supernatant were concentrated by ultracentrifugation and used to infect PC12 cells.

Cell culture

PC12 cells were cultured in serum-DME as described previously (Fath et al., 2002). For stable lines, 250 µg/ml Geneticin was included in the medium. Undifferentiated cells were plated on 35-mm polylysine- and collagen-coated glass-bottom culture dishes (MatTek Corporation) at 10^3 cells/cm^2 and cultured in DME with 1% (vol/vol) serum. Cells were flattened by addition of 100 ng/ml 7S mouse NGF (Alomone Laboratories) for 1–2 d. For neuronal differentiation, NGF treatment was extended to 4–6 d and the medium was changed every 2–3 d. Before imaging, the medium was exchanged against the same medium containing DME without Phenol red. For some experiments, cells were treated with 10 nM BAPTA/AM (EMD) for 30 min before imaging.

Primary cortical cultures were prepared from cerebral cortices of mouse embryos (day 15–17 of gestation) and cultured as described previously (Leschik et al., 2007). The cultures were obtained by breeding C57BL/6 mice. Cells were plated at 5×10^4 cells/cm^2 on polylysine- and laminin-coated coverslips.

Immunocytochemistry

Immunocytochemistry after fixation with 4% paraformaldehyde and a combined NP-40 detergent extraction–fixation procedure to reveal cytoskeletal association were performed as described previously (Brandt et al., 1995). Fluorescence microscopy was performed using a dry 20× (NA 0.45; ELWD), an oil-immersion 60× (NA 1.4), and an oil-immersion 100× (NA 1.3)

objective lens on a fluorescence microscope (Eclipse TE2000-U; Nikon) equipped with a digital camera (COOL-1300; Vosskühler). Image analysis used the program Lucia G version 4.60 (Nikon).

Photoactivation and live imaging

Live imaging was performed on a laser scanning microscope (Eclipse TE2000-U inverted; Nikon) equipped with argon (488 nm), helium/neon (543 nm) and blue diode (405 nm) lasers. PAGFP-expressing cells were visualized with a Fluor 60× (NA 1.4) UV-corrected (VC) objective lens. The microscope was enclosed in an incubation chamber maintained at 37°C and 5% CO_2 (Solent Scientific Limited). Automated image acquisition after photoactivation was essentially performed as described previously (Weissmann et al., 2009). Photoactivation was performed with the blue diode producing an activation spot 5 µm in diameter. Frames were obtained at a frequency of 1 frame/s or 1 frame/12 s, and 112 frames were collected per experiment. Standard series were collected at a resolution of 256 × 256 pixels. For higher resolution imaging, images were collected at 512 × 512 pixels with a frame frequency of one frame every 3 s. Live cell imaging of EGFP-expressing cell lines was performed by acquiring images of single cells at a resolution of 512 × 512 pixels at 488 nm. Cells were relocated at different days with the help of gridded incubation chambers. Determination of process numbers and length was performed using EZ-C1 software (Nikon).

Image analysis and modeling

Image analysis of photoactivation experiments was performed essentially as described previously (Weissmann et al., 2009). To provide a visual representation of the distribution over time, data were plotted as a color-coded filled contour plot of 2D intensity function. To compare the distribution of different constructs, I_t/I_{tot} from the fluorescence intensity at time t after activation in the activated segment and the fluorescence signal from total photoactivation were determined. This value reflects the immobile fraction of the activated population in the activated segment at time t. Effective diffusion coefficients were determined by using a diffusion model solving Fick's second diffusion equation and fitting the data from the photoactivation experiments as described previously (Weissmann et al., 2009).

shRNA treatment of cultures

PC12 cells stably expressing PAGFP-wt tau or R406W tau were plated on 35-mm dishes. After 24 h, medium was exchanged to serum-DME containing 5 µg/ml hexadimethrine bromide to neutralize charge interactions and to increase binding between the pseudoviral capsid and the cellular membrane. Lentiviral particles coding for AnxA2 shRNA or a scrambled shRNA sequence as a control (Santa Cruz Biotechnology, Inc.) were thawed at room temperature, gently mixed before use, and added to the culture. After overnight exposure at 37°C and 5% CO_2, medium was exchanged against serum-DME. Tau-expressing stable lines were additionally treated with 250 µg/ml Geneticin. To select stable clones expressing the AnxA2 shRNA or the control shRNA, cells were split on the next day 1:4 and incubated for another 24 h in serum-DME. Selection was performed with 5 µg/ml puromycin dihydrochloride (Acros Organics). Medium was replaced with fresh Geneticin- and puromycin-containing medium every 3–4 d. 6 d after infection, NGF treatment with 100 ng/ml 7S mouse NGF was started and continued for 4 d. Cells were analyzed 10 d after infection. For immunoblotting, cell lysate was prepared in RIPA buffer (50 mM Tris-HCl, 150 mM NaCl, 2 mM EDTA, 1% NP-40, 0.5% deoxycholate, and 0.1% SDS, pH 8.0) containing protease inhibitors (1 mM PMSF, 10 µg/ml leupeptin, 10 µg/ml pepstatin, and 1 mM EGTA).

Microsphere separation of the membrane cortex

Microsphere separation of the neural membrane cortex was performed from PC12 cells stably expressing wt tau or R406W tau as described previously (Maas et al., 2000). PC12 cells stably transfected with FLAG-wt tau or FLAG-R406W tau were surface labeled with sulfosuccinimidyl 2-(biotinamido)ethyl-1,3'-dithiopropionate (Pierce) and incubated with streptavidin-coated microspheres. Cellular homogenates were prepared by freeze-thawing the scraped-off cells in a separation buffer (0.25 M sucrose containing 1 mM ATP, 1 mM MgCl$_2$, 1 mM EGTA, and protease and phosphatase inhibitors), and the plasma membrane/membrane cortex fraction (PM) was separated with a magnetic bead attractor. The unbound material was separated by ultracentrifugation into an organelle/membrane pellet and a cytosol fraction (Fig. 4 A).

TAP and mass spectrometric analyses

A tau expression vector was generated by site-specific recombination (Gateway; Invitrogen) of the PCR-amplified 441 tau open reading frame into the MoMLV-based vector pZome1 (Cellzome; Euroscarf GmbH).

Pools of SKNBE2 cells stably expressing TAP-tagged full-length tau were generated by viral transduction as described previously (Brajenovic et al., 2004). TAP and MS procedures were performed as described previously (Brajenovic et al., 2004). In brief, cell lysates were incubated with IgG agarose, and the beads were collected, washed, and incubated with tobacco etch virus protease. The eluate was transferred into a column containing calmodulin agarose and the column was eluted with 600 µl elution buffer (10 mM Tris-HCl and 5 mM EGTA, pH 8.0). Samples were separated on 4–12% NuPAGE gels and stained with colloidal Coomassie. Gels were cut across the entire separation range of each lane to sample all proteins without bias with respect to size and relative abundance. Cut bands were reduced, alkylated, and digested, and peptides were sequenced by tandem MS (LC-MS/MS, QTOF Ultima, and CapLC; Waters). Most proteins were unambiguously identified by the sequencing of several independent peptides.

Expression of tau and annexin in yeast
Recombinant 352 and 441 tau variants were expressed with an amino-terminal FLAG-tag in the yeast strain DHD5 (Kirchrath et al., 2000) from episomal vectors based on YEp352 (2 µm, $URA3 \rightarrow$ pJJH447) under the control of the $GAL1/10$ promoter. The coding sequence for an AnxA2–GFP fusion protein was expressed under the control of the constitutive $PFK2$ promoter from a vector based on YEplac181 (2 µm, $LEU2 \rightarrow$ pJJH216). Transformants were grown on synthetic minimal media selecting for plasmid maintenance and using 2% galactose as a carbon source for high-level expression of the tau constructs.

GFP pull-down assays
Yeast extracts were prepared from yeast cells expressing recombinant GFP–AnxA2 and wt tau or R406W tau (352 and 441) in Ca^{2+}-containing lysis buffer (10 mM Tris-HCl, 150 mM NaCl, 0.15% NP-40, and 1 mM $CaCl_2$, pH 7.5) by vigorous shaking with glass beads for 7 min at 4°C. In all cases, the buffer also contained protease and phosphatase inhibitors (1 mM PMSF, 10 µg/ml leupeptin, 10 µg/ml pepstatin, 1 mM sodium orthovanadate, 20 mM sodium fluoride, and 1 mM sodium pyrophosphate). GFP-Trap_A beads (ChromoTek) were equilibrated in 500 µl ice-cold immunoprecipitation (IP) buffer (10 mM Tris-HCl, 150 mM NaCl, and 1 mM PMSF, pH 7.5) containing 1 mM $CaCl_2$. Lysates were diluted to 500 µl with IP buffer, and 10% were saved ("input" fraction). The remaining lysate was incubated with the equilibrated GFP-Trap_A beads by end-over-end mixing for 2 h at 4°C. GFP or GFP fusion proteins were pulled-down by centrifugation at 2,000 g for 2 min at 4°C. For immunoblot analysis, 50 µl of the supernatant were saved ("supernat." fraction in Fig. 7 B). The pellet was washed twice with ice-cold IP buffer, resuspended in 100 µl 2× SDS-sample buffer, and boiled for 10 min at 95°C to dissociate the immunocomplexes from the beads. Beads were collected by centrifugation at 2,700 g for 2 min at 4°C, and the supernatant was saved ("GFP pull down" fraction in Fig. 7 B). For SDS-PAGE, 2% of the lysate ("input" in Fig. 7 B) and 10% each of the "supernat." and "GFP pull down" fraction were loaded.

Other methods
Immunoblot analysis and quantification of the blots were performed as described previously (Leschik et al., 2007). Data were expressed as means ± SEM. Statistical analysis among experimental groups was performed using a paired Student's t test (Origin 7.0) or one-way analysis of variance (ANOVA) followed by a post-hoc Bonferroni test. P-values are *, $P < 0.05$; **, $P < 0.01$; and ***, $P < 0.001$.

References

Aoyagi, H., M. Hasegawa, and A. Tamaoka. 2007. Fibrillogenic nuclei composed of P301L mutant tau induce elongation of P301L tau but not wild-type tau. *J. Biol. Chem.* 282:20309–20318. doi:10.1074/jbc.M611876200

Biernat, J., N. Gustke, G. Drewes, E.M. Mandelkow, and E. Mandelkow. 1993. Phosphorylation of Ser262 strongly reduces binding of tau to microtubules: distinction between PHF-like immunoreactivity and microtubule binding. *Neuron.* 11:153–163. doi:10.1016/0896-6273(93)90279-Z

Brajenovic, M., G. Joberty, B. Küster, T. Bouwmeester, and G. Drewes. 2004. Comprehensive proteomic analysis of human Par protein complexes reveals an interconnected protein network. *J. Biol. Chem.* 279:12804–12811. doi:10.1074/jbc.M312171200

Brandt, R., J. Léger, and G. Lee. 1995. Interaction of tau with the neural plasma membrane mediated by tau's amino-terminal projection domain. *J. Cell Biol.* 131:1327–1340. doi:10.1083/jcb.131.5.1327

Bunker, J.M., K. Kamath, L. Wilson, M.A. Jordan, and S.C. Feinstein. 2006. FTDP-17 mutations compromise the ability of tau to regulate microtubule dynamics in cells. *J. Biol. Chem.* 281:11856–11863. doi:10.1074/jbc.M509420200

Busciglio, J., A. Lorenzo, J. Yeh, and B.A. Yankner. 1995. beta-amyloid fibrils induce tau phosphorylation and loss of microtubule binding. *Neuron.* 14:879–888. doi:10.1016/0896-6273(95)90232-5

Chang, E., S. Kim, H. Yin, H.N. Nagaraja, and J. Kuret. 2008. Pathogenic missense MAPT mutations differentially modulate tau aggregation propensity at nucleation and extension steps. *J. Neurochem.* 107:1113–1123.

Connell, J.W., G.M. Gibb, J.C. Betts, W.P. Blackstock, J. Gallo, S. Lovestone, M. Hutton, and B.H. Anderton. 2001. Effects of FTDP-17 mutations on the in vitro phosphorylation of tau by glycogen synthase kinase 3beta identified by mass spectrometry demonstrate certain mutations exert long-range conformational changes. *FEBS Lett.* 493:40–44. doi:10.1016/S0014-5793(01)02267-0

Cruz, J.C., and L.H. Tsai. 2004. Cdk5 deregulation in the pathogenesis of Alzheimer's disease. *Trends Mol. Med.* 10:452–458. doi:10.1016/j.molmed.2004.07.001

Dayanandan, R., M. Van Slegtenhorst, T.G. Mack, L. Ko, S.H. Yen, K. Leroy, J.P. Brion, B.H. Anderton, M. Hutton, and S. Lovestone. 1999. Mutations in tau reduce its microtubule binding properties in intact cells and affect its phosphorylation. *FEBS Lett.* 446:228–232. doi:10.1016/S0014-5793(99)00222-7

DeTure, M., L.W. Ko, S.H. Yen, P. Nacharaju, C. Easson, J. Lewis, M. van Slegtenhorst, M. Hutton, and S.H. Yen. 2000. Missense tau mutations identified in FTDP-17 have a small effect on tau-microtubule interactions. *Brain Res.* 853:5–14. doi:10.1016/S0006-8993(99)02124-1

DeTure, M., L.W. Ko, C. Easson, and S.H. Yen. 2002. Tau assembly in inducible transfectants expressing wild-type or FTDP-17 tau. *Am. J. Pathol.* 161:1711–1722. doi:10.1016/S0002-9440(10)64448-3

Dittgen, T., A. Nimmerjahn, S. Komai, P. Licznerski, J. Waters, T.W. Margrie, F. Helmchen, W. Denk, M. Brecht, and P. Osten. 2004. Lentivirus-based genetic manipulations of cortical neurons and their optical and electrophysiological monitoring in vivo. *Proc. Natl. Acad. Sci. USA.* 101:18206–18211. doi:10.1073/pnas.0407976101

Drubin, D., S. Kobayashi, D. Kellogg, and M. Kirschner. 1988. Regulation of microtubule protein levels during cellular morphogenesis in nerve growth factor-treated PC12 cells. *J. Cell Biol.* 106:1583–1591. doi:10.1083/jcb.106.5.1583

Eberhard, D.A., M.D. Brown, and S.R. VandenBerg. 1994. Alterations of annexin expression in pathological neuronal and glial reactions. Immunohistochemical localization of annexins I, II (p36 and p11 subunits), IV, and VI in the human hippocampus. *Am. J. Pathol.* 145:640–649.

Eidenmüller, J., T. Fath, T. Maas, M. Pool, E. Sontag, and R. Brandt. 2001. Phosphorylation-mimicking glutamate clusters in the proline-rich region are sufficient to simulate the functional deficiencies of hyperphosphorylated tau protein. *Biochem. J.* 357:759–767. doi:10.1042/0264-6021:3570759

Fath, T., J. Eidenmüller, and R. Brandt. 2002. Tau-mediated cytotoxicity in a pseudohyperphosphorylation model of Alzheimer's disease. *J. Neurosci.* 22:9733–9741.

Foster, N.L., K. Wilhelmsen, A.A. Sima, M.Z. Jones, C.J. D'Amato, and S. Gilman; Conference Participants. 1997. Frontotemporal dementia and parkinsonism linked to chromosome 17: a consensus conference. *Ann. Neurol.* 41:706–715. doi:10.1002/ana.410410606

Fox, M.T., D.A. Prentice, and J.P. Hughes. 1991. Increases in p11 and annexin II proteins correlate with differentiation in the PC12 pheochromocytoma. *Biochem. Biophys. Res. Commun.* 177:1188–1193. doi:10.1016/0006-291X(91)90666-U

Gerke, V., and S.E. Moss. 1997. Annexins and membrane dynamics. *Biochim. Biophys. Acta.* 1357:129–154. doi:10.1016/S0167-4889(97)00038-4

Gerke, V., and S.E. Moss. 2002. Annexins: from structure to function. *Physiol. Rev.* 82:331–371.

Gerke, V., C.E. Creutz, and S.E. Moss. 2005. Annexins: linking Ca2+ signalling to membrane dynamics. *Nat. Rev. Mol. Cell Biol.* 6:449–461. doi:10.1038/nrm1661

Götz, J., and L.M. Ittner. 2008. Animal models of Alzheimer's disease and frontotemporal dementia. *Nat. Rev. Neurosci.* 9:532–544. doi:10.1038/nrn2420

Greene, L.A., M.M. Sobeih, and K.K. Teng. 1991. Methodologies for the culture and experimental use of the PC12 rat pheochromocytoma cell line. *In* Culturing Nerve Cells. G. Banker and K. Goslin, editors. MIT Press, Cambridge, Massachusetts. 207–226.

Hooper, C., R. Killick, and S. Lovestone. 2008. The GSK3 hypothesis of Alzheimer's disease. *J. Neurochem.* 104:1433–1439. doi:10.1111/j.1471-4159.2007.05194.x

Ikeuchi, T., H. Kaneko, A. Miyashita, H. Nozaki, K. Kasuga, T. Tsukie, M. Tsuchiya, T. Imamura, H. Ishizu, K. Aoki, et al. 2008. Mutational analysis in early-onset familial dementia in the Japanese population. The role of PSEN1 and MAPT R406W mutations. *Dement. Geriatr. Cogn. Disord.* 26:43–49. doi:10.1159/000141483

Jacovina, A.T., F. Zhong, E. Khazanova, E. Lev, A.B. Deora, and K.A. Hajjar. 2001. Neuritogenesis and the nerve growth factor-induced differentiation of PC-12 cells requires annexin II-mediated plasmin generation. *J. Biol. Chem.* 276:49350–49358. doi:10.1074/jbc.M106289200

Jeganathan, S., M. von Bergen, H. Brutlach, H.J. Steinhoff, and E. Mandelkow. 2006. Global hairpin folding of tau in solution. *Biochemistry*. 45:2283–2293. doi:10.1021/bi0521543

Kirchrath, L., A. Lorberg, H.P. Schmitz, U. Gengenbacher, and J.J. Heinisch. 2000. Comparative genetic and physiological studies of the MAP kinase Mpk1p from *Kluyveromyces lactis* and *Saccharomyces cerevisiae. J. Mol. Biol.* 300:743–758. doi:10.1006/jmbi.2000.3916

Krishnamurthy, P.K., and G.V. Johnson. 2004. Mutant (R406W) human tau is hyperphosphorylated and does not efficiently bind microtubules in a neuronal cortical cell model. *J. Biol. Chem.* 279:7893–7900. doi:10.1074/jbc.M311203200

Leschik, J., A. Welzel, C. Weissmann, A. Eckert, and R. Brandt. 2007. Inverse and distinct modulation of tau-dependent neurodegeneration by presenilin 1 and amyloid-beta in cultured cortical neurons: evidence that tau phosphorylation is the limiting factor in amyloid-beta-induced cell death. *J. Neurochem.* 101:1303–1315. doi:10.1111/j.1471-4159.2006.04435.x

Leugers, C.J., and G. Lee. 2010. Tau potentiates nerve growth factor-induced mitogen-activated protein kinase signaling and neurite initiation without a requirement for microtubule binding. *J. Biol. Chem.* 285:19125–19134. doi:10.1074/jbc.M110.105387

Lindquist, S.G., I.E. Holm, M. Schwartz, I. Law, M. Stokholm, M. Batbayli, G. Waldemar, and J.E. Nielsen. 2008. Alzheimer disease-like clinical phenotype in a family with FTDP-17 caused by a MAPT R406W mutation. *Eur. J. Neurol.* 15:377–385. doi:10.1111/j.1468-1331.2008.02069.x

Maas, T., J. Eidenmüller, and R. Brandt. 2000. Interaction of tau with the neural membrane cortex is regulated by phosphorylation at sites that are modified in paired helical filaments. *J. Biol. Chem.* 275:15733–15740. doi:10.1074/jbc.M000389200

Matsumura, N., T. Yamazaki, and Y. Ihara. 1999. Stable expression in Chinese hamster ovary cells of mutated tau genes causing frontotemporal dementia and parkinsonism linked to chromosome 17 (FTDP-17). *Am. J. Pathol.* 154:1649–1656. doi:10.1016/S0002-9440(10)65420-X

Miyasaka, T., M. Morishima-Kawashima, R. Ravid, P. Heutink, J.C. van Swieten, K. Nagashima, and Y. Ihara. 2001. Molecular analysis of mutant and wild-type tau deposited in the brain affected by the FTDP-17 R406W mutation. *Am. J. Pathol.* 158:373–379. doi:10.1016/S0002-9440(10)63979-X

Morgan, R.O., and M.P. Fernández. 1997. Annexin gene structures and molecular evolutionary genetics. *Cell. Mol. Life Sci.* 53:508–515. doi:10.1007/s000180050064

Ostojic, J., C. Elfgren, U. Passant, K. Nilsson, L. Gustafson, L. Lannfelt, and S. Froelich Fabre. 2004. The tau R406W mutation causes progressive presenile dementia with bitemporal atrophy. *Dement. Geriatr. Cogn. Disord.* 17:298–301. doi:10.1159/000077158

Patterson, G.H., and J. Lippincott-Schwartz. 2002. A photoactivatable GFP for selective photolabeling of proteins and cells. *Science*. 297:1873–1877. doi:10.1126/science.1074952

Piperno, G., M. LeDizet, and X.J. Chang. 1987. Microtubules containing acetylated alpha-tubulin in mammalian cells in culture. *J. Cell Biol.* 104:289–302. doi:10.1083/jcb.104.2.289

Rescher, U., and V. Gerke. 2004. Annexins—unique membrane binding proteins with diverse functions. *J. Cell Sci.* 117:2631–2639. doi:10.1242/jcs.01245

Rizzu, P., J.C. Van Swieten, M. Joosse, M. Hasegawa, M. Stevens, A. Tibben, M.F. Niermeijer, M. Hillebrand, R. Ravid, B.A. Oostra, et al. 1999. High prevalence of mutations in the microtubule-associated protein tau in a population study of frontotemporal dementia in the Netherlands. *Am. J. Hum. Genet.* 64:414–421. doi:10.1086/302256

Schlaepfer, D.D., and H.T. Haigler. 1990. Expression of annexins as a function of cellular growth state. *J. Cell Biol.* 111:229–238. doi:10.1083/jcb.111.1.229

Spillantini, M.G., R.A. Crowther, and M. Goedert. 1996. Comparison of the neurofibrillary pathology in Alzheimer's disease and familial presenile dementia with tangles. *Acta Neuropathol.* 92:42–48. doi:10.1007/s004010050487

Sprague, B.L., R.L. Pego, D.A. Stavreva, and J.G. McNally. 2004. Analysis of binding reactions by fluorescence recovery after photobleaching. *Biophys. J.* 86:3473–3495. doi:10.1529/biophysj.103.026765

Stoothoff, W.H., and G.V. Johnson. 2005. Tau phosphorylation: physiological and pathological consequences. *Biochim. Biophys. Acta*. 1739:280–297.

Tackenberg, C., and R. Brandt. 2009. Divergent pathways mediate spine alterations and cell death induced by amyloid-beta, wild-type tau, and R406W tau. *J. Neurosci.* 29:14439–14450. doi:10.1523/JNEUROSCI.3590-09.2009

Thiel, C., M. Osborn, and V. Gerke. 1992. The tight association of the tyrosine kinase substrate annexin II with the submembranous cytoskeleton depends on intact p11- and Ca(2+)-binding sites. *J. Cell Sci.* 103:733–742.

Vogelsberg-Ragaglia, V., J. Bruce, C. Richter-Landsberg, B. Zhang, M. Hong, J.Q. Trojanowski, and V.M. Lee. 2000. Distinct FTDP-17 missense mutations in tau produce tau aggregates and other pathological phenotypes in transfected CHO cells. *Mol. Biol. Cell*. 11:4093–4104.

Weissmann, C., H.J. Reyher, A. Gauthier, H.J. Steinhoff, W. Junge, and R. Brandt. 2009. Microtubule binding and trapping at the tip of neurites regulate tau motion in living neurons. *Traffic*. 10:1655–1668. doi:10.1111/j.1600-0854.2009.00977.x

Yoshiyama, Y., V.M. Lee, and J.Q. Trojanowski. 2001. Frontotemporal dementia and tauopathy. *Curr. Neurol. Neurosci. Rep.* 1:413–421. doi:10.1007/s11910-001-0100-0

Zhang, B., M. Higuchi, Y. Yoshiyama, T. Ishihara, M.S. Forman, D. Martinez, S. Joyce, J.Q. Trojanowski, and V.M. Lee. 2004. Retarded axonal transport of R406W mutant tau in transgenic mice with a neurodegenerative tauopathy. *J. Neurosci.* 24:4657–4667. doi:10.1523/JNEUROSCI.0797-04.2004